Active carbody roll control in railway vehicles using hydraulic actuation

Edoardo F. Colombo, Egidio Di Gialleonardo, Alan Facchinetti, Stefano Bruni *

Dipartimento di Meccanica, Politecnico di Milano, Via La Masa, 1 I-20156 Milan, Italy

Received 1 October 2013 Accepted 30 May 2014

1. Introduction

Recent decades have seen increasing integration of electronics and control into rail vehicles which used to be purely mechanical systems (Goodall, 2011). As part of this process, mechatronic technologies are increasingly being introduced in the running gear to improve running dynamics, service performance and ride quality (Bruni, Goodall, Mei, & Tsunashima, 2007; Goodall, Bruni, & Facchinetti, 2012).

In this regard, particularly noteworthy is the development of concepts for active secondary suspension (i.e. the suspension stage that isolates the carbody from the bogies (Goodall et al., 2012)), with the aim of raising service speeds on existing networks with the same level of ride comfort. Tilting carbody technology is an obvious example of this trend, but requires a rather complex bogie and suspension design based on a tilting bolster (Persson, Goodall, & Sasaki, 2009), which leads to increased vehicle weight and, given the constraints applied to the vehicle gauge, reduces the space available for passengers.

For these reasons, tilting body technology in the strict sense is not used for very high-speed trains, where severe constraints apply in terms of maximum axle load. For this specific application simpler and lighter carbody roll actuation systems have been proposed, aiming at permitting limited tilt angles (in the range of 1–2°, compared with the 6–8° maximum tilt angle achieved by tilting trains in the strict sense) that are nevertheless sufficient to increase service speed significantly on existing lines.

An example of this concept is the Japanese high-speed train Shinkansen Series N700, which attains approximately 1° tilting by actively controlling the pneumatic secondary suspension (Nakakura & Hayakawa, 2009; Tanifuji, Koizumi, & Shimamune, 2002). The same concept was proposed in Alfi, Bruni, Diana, Facchinetti, and Mazzola (2011), also showing the possible use of active roll actuation to reduce overturning risk in the presence of crosswind. Pneumatic actuation via secondary air springs is, however, not free from drawbacks: firstly, the actuation pass-band is limited, which may lead to delays in tracking the desired tilt reference. Secondly, the coupling of vertical and roll carbody motion and the dynamics of the pneumatic system cause disturbances affecting ride comfort and potentially leading to instability problems (Facchinetti, Di Gialleonardo, Resta, Bruni, & Brundisch, 2011; Tanifuji, Saito, Soma, Ishii, & Kajitani, 2009). Thirdly, with this actuation concept the use of a mechanical anti-roll bar cannot be avoided and the restoring roll torque generated by this component counteracts roll actuation, resulting in smaller tilt angles and increased energy consumption (Facchinetti et al., 2011).

This paper proposes an active anti-roll device to replace the passive anti-roll bar, making it possible actively to tilt the carbody.

* Corresponding author.
E-mail address: stefano.bruni@polimi.it (S. Bruni).

The use of an active anti-roll bar in rail vehicles was first suggested by Pearson, Goodall, and Pratt (1998), with a modified layout of a mechanical bar in which either linear actuators were introduced to replace the links to the carbody, or a rotary actuator was placed in series with the torsion bar. This original concept, however, is difficult to make fault tolerant, which is a major drawback. For this reason, in this paper hydraulic actuation is proposed instead, using cross-connected actuators so that a roll torque can be generated for a theoretically null vertical force: in this way it is easier to reject track irregularity related disturbances and, at the same time, tilt actuation becomes faster, more accurate and less energy consuming compared with pneumatic actuation. The hydraulic system can be dimensioned to provide the same roll stiffness as a conventional anti-roll bar when operated in the passive mode (Colombo, Di Gialleonardo, Facchinetti, & Bruni, 2013).

Three different control strategies are proposed for the active hydraulic anti-roll device and for all three control gains are defined based on Genetic Algorithm (GA) optimisation, having as multiple objectives the tracking of a reference carbody tilt angle, optimising ride comfort and keeping the energy required for actuation within acceptable limits. The reference tilt angle is defined on the basis of vehicle speed and curve geometry (curvature, cant, length of transitions), under the assumption that this information is made available to the control unit through geo-localisation of the train and mapping of the line, as implemented in the Shinkansen N700 train (Nakakura & Hayakawa, 2009). Other ways of defining the reference tilt angle, i.e. based on inertial sensors, would be possible and are in use, but it is not the purpose of this paper to investigate or discuss the benefits and drawbacks of alternative methods available to accomplish this task.

2. Concept of the active hydraulic anti-roll device

The active anti-roll device is designed to accomplish two main functions:

- actuate the desired carbody tilt angle when the vehicle negotiates a curve;
- provide the same carbody to bogie roll stiffness as a conventional anti-roll bar device when carbody tilt is not required.

A scheme of the device is shown in Fig. 1 for one bogie and includes the following main components:

- two linear hydraulic actuators AL and AR, placed at the left and right side of the bogie and connecting the bogie frame with the carbody;

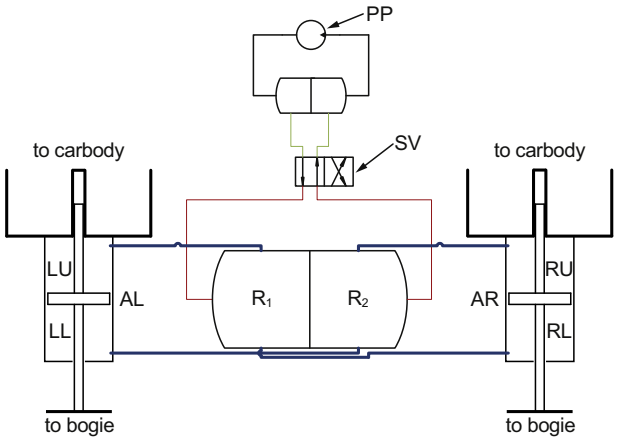

Fig. 1. Scheme of the hydraulic anti-roll device.

- a main hydraulic circuit (thick solid lines in the figure), cross-connecting the chambers of the actuators. Two reservoirs R1 and R2 are introduced in the circuit, and their volume is designed to provide the desired degree of roll compliance in passive mode;
- a hydraulic feeder circuit (thin solid line in the figure) to control fluid flow in the reservoirs with a pump (PP) and a servo-valve SV.

The working principle in passive mode is the same as for hydraulically interconnected suspensions developed mainly for automotive applications (Zhang, Smith, & Jeyakumaran, 2010). The upper chamber of the left actuator (LU) is connected to the lower chamber of the right actuator (RL) and the lower chamber of the left actuator (LL) with the upper chamber of the right actuator (RU). In this way, the hydraulic suspension nominally provides zero stiffness in the vertical direction and a non-zero roll stiffness.

A slow upward bouncing movement of the carbody will reduce the oil volume in the two upper chambers LU and RU and will increase the volume in the two lower chambers LL and RL by the same amount. Thanks to the cross-connection of the chambers, oil will flow from LU to RL and from RU to LL and, neglecting viscosity effects, no variation of the pressure in the chambers will occur. In a slow downward bouncing motion of the carbody, oil will flow from LL to RU and from RL to LU and again no pressure variation and hence no vertical force will be generated.

When instead the carbody performs a roll rotation with respect to the bogie for example counter-clockwise, the volumes in chambers LL and RU will decrease while those in LU and RL will increase. As a consequence, oil pressure will increase in LL and RU and decrease in LU and RL, producing a restoring moment in the roll direction.

The active roll function is only activated during curve negotiation and is implemented by the actuated servo-valve SV which controls the volume of oil in the two branches of the main hydraulic circuit, extending the linear actuator on one side while contracting the other actuator, thus providing carbody tilt. The reference carbody tilt angle is defined based on the cant deficiency of the curve which, in turn, depends on the curve geometry and on the vehicle speed. The position of the vehicle along the curve is assumed to be known from a positioning system, in the same way as in Nakakura and Hayakawa (2009).

The active hydraulic anti-roll device is used in conjunction with an active hydraulic secondary lateral suspension, whose function is to reduce the unloading of the inner wheels caused by the lateral displacement of the carbody and to prevent the lateral bump-stops to come in contact with the carbody, which would degrade ride quality. The active lateral suspension envisaged here is a simple “hold-off” type (Bruni et al., 2007), generating a lateral force in open loop which is defined to be proportional to the cant deficiency. Because of the simple control strategy envisaged for the active lateral suspension, the integration of active tilt and active lateral control at the secondary suspension as proposed in Zhou, Zolotas, and Goodall (2011) is not pursued here.

3. Mathematical model

A detailed non-linear model of the active hydraulic anti-roll device was derived and interfaced with a non-linear mechanical model of the entire rail vehicle, to optimise the controller parameters using the Genetic Algorithm and to assess numerically the performance of the actuated vehicle.

3.1. Model of the active hydraulic anti-roll bar

The following assumptions were made in developing a mathematical model of the hydraulic anti-roll bar:

(i) laminar and mono-dimensional flow in all pipes, losses due to fluid viscosity are neglected;
(ii) isothermal conditions of the fluid;
(iii) partially compressible fluid in the actuator chambers;
(iv) incompressible fluid in the pipes and reservoir;
(v) constant values for the supply and return pressures;
(vi) negligible inertial effects in the piston and piston rod;
(vii) servo-valve assumed to behave as a 1st order system.

Based on assumptions (i)–(vii), a 3rd order model is derived for the active suspension. Two state variables are introduced for the fluid pressure p_1 in reservoir R1 and chambers RU and LL, and the fluid pressure p_2 in reservoir R2 and chambers LU and RL. The third state variable, x_s, is the position of the spool in the servo-valve.

Considering conservation of mass for the fluid volume contained in each branch of the main hydraulic circuit and considering assumptions (i)–(iv), the following state equations are obtained (details are provided in Appendix A):

$$\left(\frac{2V_0}{\beta}+\frac{A(u_r-u_l)}{\beta}\right)\dot{p}_1+2(c_i+c_e)p_1-2c_ip_2=-A(\dot{u}_r-\dot{u}_l)+Q_{s_1} \tag{1}$$

$$\left(\frac{2V_0}{\beta}-\frac{A(u_r-u_l)}{\beta}\right)\dot{p}_2-2c_ip_1+2(c_i+c_e)p_2=+A(\dot{u}_r-\dot{u}_l)+Q_{s_2} \tag{2}$$

where V_0 is the total fluid volume contained in each branch of the main circuit when the suspension is in the reference position, β is the bulk modulus, A is the area of the piston, u_l and u_r are the displacements of the piston in the left and right actuators, c_i and c_e are the internal and external leakage coefficient of the piston (Merritt, 1967) and, finally, Q_{s_1} and Q_{s_2} are the volumetric flow rates corresponding to an inlet/outlet of fluid produced by the servo-valve in the two branches of the circuit (see Fig. A1). The flow rate quantities Q_{s_1} and Q_{s_2} are non-linearly dependent on the pressure drop across the servo-valve and on the position x_s of the servo-valve spool:

$$Q_{s_{1,2}}=\begin{cases} C_s(x_s)d_sx_s\sqrt{\frac{2(p_S-p_{1,2})}{\rho}} & \text{for fluid supply} \\ -C_s(x_s)d_sx_s\sqrt{\frac{2(p_{1,2}-p_R)}{\rho}} & \text{for fluid return} \end{cases} \tag{3}$$

with p_S and p_R the supply and return pressure in the feeding circuit, C_s the efflux coefficient, which varies with the position of the spool, and d_s a constant length parameter characteristic of the servo-valve.

The servo-valve dynamics is described by the 1st order equation:

$$\dot{x}_s+\frac{1}{\tau_s}x_s=\frac{k_s}{\tau_s}u_s \tag{4}$$

with u_s the command to the servo-valve, τ_s the time constant of the servo-valve and k_s a characteristic gain of the servovalve.

Replacing Eq. (3) in (1) and (2) and adding Eq. (4) a set of non-linear 3rd-order state equations is obtained, which describes the pressure variations in the two branches of the circuit as functions of the actuators' displacements u_l and u_r (applied by the vehicle, see Section 3.2) and of command u_s (defined by the regulator, see Section 4).

The forces generated on the left and right pistons are finally defined as:

$$\begin{aligned} F_l&=-A(p_1-p_2) \\ F_r&=A(p_1-p_2) \end{aligned} \tag{5}$$

3.2. Model of the actuated vehicle

The active suspension model described in Section 3.1 was interfaced with a multi-body model of a complete rail vehicle which was defined using the in-house developed simulation software ADTreS (Bruni, Collina, Diana, & Vanolo, 1999; Di Gialleonardo, Braghin, & Bruni, 2012). The rail vehicle model consists of one carbody, two bogies and four wheelsets, all considered as rigid bodies, and of primary and secondary vehicle suspensions, modelled as linear and non-linear lumped parameter elastic and viscous elements.

Each rigid body is assigned five degrees of freedom (vertical and lateral displacements, yaw, roll and pitch rotations), while the forward motion of the body's centre of mass is assumed to have constant speed V. Therefore, the model has a total of 35 degrees of freedom.

Wheel–rail contact forces are introduced according to a non-linear multi-Hertzian contact model (Braghin, Bruni, & Diana, 2006). Excitation introduced by track irregularity is introduced in the simulation by considering a time history of vertical and lateral displacements applied to the contact points on the rails, according to a random irregularity profile generated based on the ERRI spectra for track irregularities considering the low level irregularity case (ERRI: B176/3, 1993). Track flexibility effects are not considered in the simulation, as these would mainly affect the high-frequency component of the vehicle dynamics (above 20 Hz) (Di Gialleonardo et al., 2012), whereas the interest here lies in the frequency range up to 5–10 Hz.

The motion of each body is described with respect to a moving reference travelling with constant speed along the track centre-line. The bodies are assumed to undergo small displacements relative to the moving reference so that the equations of motion for the vehicle can be linearised with respect to kinematical non-linear effects only, and take the symbolic form:

$$\mathbf{M}_v\ddot{\mathbf{z}}_v+\mathbf{C}_v\dot{\mathbf{z}}_v+\mathbf{K}_v\mathbf{z}_v=\mathbf{F}_i(V,t)+\mathbf{F}_{nl}(\mathbf{z}_v,\dot{\mathbf{z}}_v)+\mathbf{F}_c(\mathbf{z}_v,\dot{\mathbf{z}}_v,V,t) \tag{6}$$

where $\mathbf{z}_v$ is the vector of the vehicle's 35 coordinates shown in Fig. 2 (yaw rotations are not depicted for the sake of clarity), $\mathbf{M}_v$, $\mathbf{C}_v$ and $\mathbf{K}_v$ are the mass, damping and stiffness matrices of the vehicle respectively, $\mathbf{F}_i$ is the vector of inertial forces due to the non-inertial motion of the moving references (this term reduces to zero when the vehicle is considered to move along a tangent track), V is the vehicle speed, $\mathbf{F}_{nl}$ is the vector of forces due to non-linear elements in the suspensions (including the active suspension considered here) and $\mathbf{F}_c$ is the vector of the generalised forces due to wheel–rail contact. More details on the derivation of the equations of motion for the vehicle can be found in Braghin et al. (2006), Bruni et al. (1999), and Di Gialleonardo et al. (2012).

A co-simulation is established between the vehicle model described by Eq. (6) and the models of the two active suspensions on the leading and trailing bogie. To this end, the piston displacements $u_l^{(l)}$, $u_r^{(l)}$, $u_l^{(t)}$ and $u_r^{(t)}$ (with superscripts l and t referring to the leading and trailing bogie respectively) are derived from the vehicle coordinates according to the following equation, see Fig. 2 for the nomenclature of geometric parameters used and for sign conventions:

$$\begin{aligned} u_l^{(l)}&=x^{(c)}+l\vartheta_y^{(c)}-b\vartheta_z^{(c)}-x^{(l)}+b\vartheta_z^{(l)} \\ u_l^{(t)}&=x^{(c)}-l\vartheta_y^{(c)}-b\vartheta_z^{(c)}-x^{(t)}+b\vartheta_z^{(t)} \\ u_r^{(l)}&=x^{(c)}+l\vartheta_y^{(c)}+b\vartheta_z^{(c)}-x^{(l)}-b\vartheta_z^{(l)} \\ u_r^{(t)}&=x^{(c)}-l\vartheta_y^{(c)}+b\vartheta_z^{(c)}-x^{(l)}-b\vartheta_z^{(l)} \end{aligned} \tag{7}$$

The time derivatives of the piston displacements are obtained by straightforward derivation with respect to time of Eq. (7).

The forces generated by the actuators of the hydraulic suspension give rise to non-zero resultant vertical forces on the carbody,

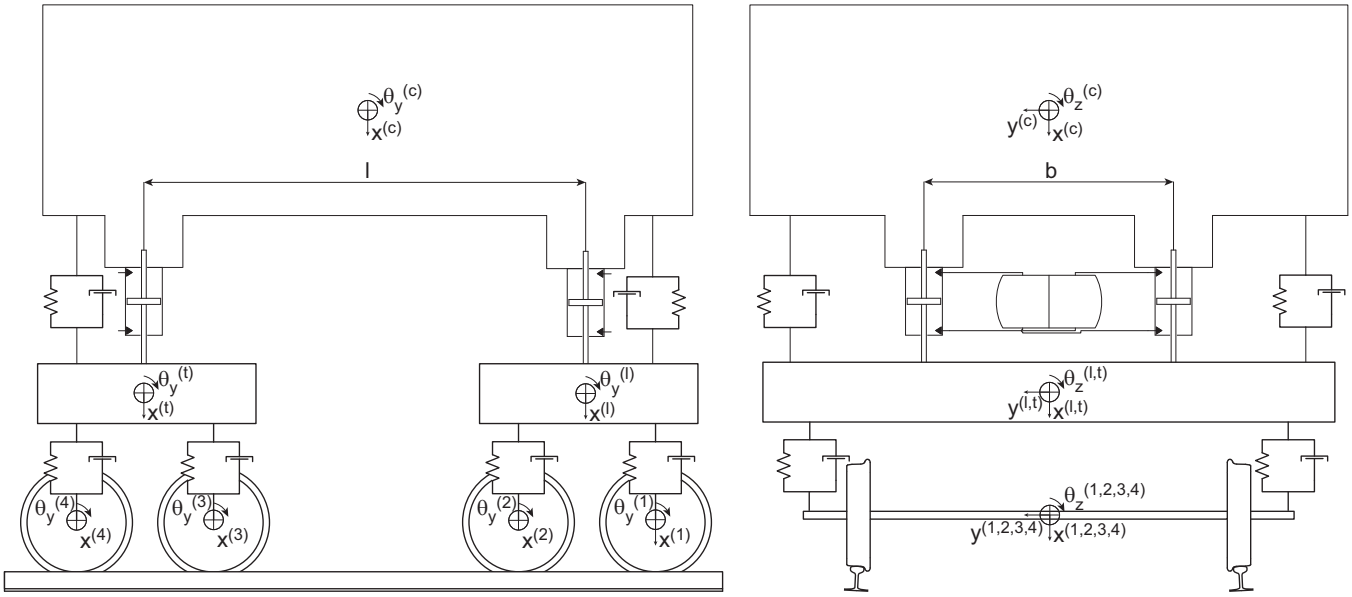

Fig. 2. Side and rear view of the actuated vehicle.

leading and trailing bogie, denoted respectively as $F_x^{(c)}$, $F_x^{(l)}$ and $F_x^{(t)}$, which are expressed as:

$$\begin{aligned} F_x^{(c)} &= -(F_l^{(l)} + F_r^{(l)} + F_l^{(t)} + F_r^{(t)}) \\ F_x^{(l)} &= F_l^{(l)} + F_r^{(l)} \\ F_x^{(t)} &= F_l^{(t)} + F_r^{(t)} \end{aligned} \tag{8}$$

where $F_{l,r}^{(l)}$ are the forces generated on the left and right side of the leading bogie and $F_{l,r}^{(t)}$ the forces generated by the suspension on the trailing bogie. Furthermore, the actuators' forces give rise to resultant roll moments on the carbody and bogies $M_z^{(c)}$, $M_z^{(l)}$ and $M_z^{(t)}$ and to a pitch moment on the carbody $M_y^{(c)}$, whose expressions are:

$$\begin{aligned} M_z^{(c)} &= \left(F_l^{(l)} - F_r^{(l)} + F_l^{(t)} - F_r^{(t)}\right) b \\ M_y^{(c)} &= \left(-F_l^{(l)} - F_r^{(l)} + F_l^{(t)} + F_r^{(t)}\right) l \\ M_z^{(l)} &= -\left(F_l^{(l)} - F_r^{(l)}\right) b \\ M_z^{(t)} &= -\left(F_l^{(t)} - F_r^{(t)}\right) b \end{aligned} \tag{9}$$

The forces and moments defined by Eqs. (8) and (9) are applied to the carbody and bogies and appear in vector $\mathbf{F}_{nl}$ of Eq. (6).

The state vector $\mathbf{x}$ and input vector $\mathbf{u}$ for the model of the actuated vehicle are defined as follows:

$$\mathbf{x} = \left\{ \mathbf{z}_v^T \quad \dot{\mathbf{z}}_v^T \quad p_1^{(l)} \quad p_2^{(l)} \quad x_s^{(l)} \quad p_1^{(t)} \quad p_2^{(t)} \quad x_s^{(t)} \right\}^T \tag{10}$$

$$\mathbf{u} = \left\{ u_s^{(l)} \quad u_s^{(t)} \right\}^T \tag{11}$$

with $p_1^{(l)}$, $p_2^{(l)}$, $x_s^{(l)}$ and $p_1^{(t)}$, $p_2^{(t)}$, $x_s^{(t)}$ the states of the active anti-roll bar on the leading and trailing bogie respectively, and $u_s^{(l)}$, $u_s^{(t)}$ the servo-valve commands of the active suspension in the two bogies. Since $\mathbf{z}_v$ is made up of 35 coordinates, the total number of states in the model is 76.

Eqs. (6)–(9) together with Eqs. (1)–(4) for the leading and trailing bogie can be rewritten in standard state form:

$$\dot{\mathbf{x}} = \mathbf{f}(\mathbf{x}) + \mathbf{g}(\mathbf{x})\mathbf{u} \tag{12}$$

Eq. (12) is integrated numerically in the time domain, leading to the simulation of the nonlinear dynamic behaviour of the complete actuated vehicle. The servo-valve commands $u_s^{(l)}$ and $u_s^{(t)}$ are defined by the regulator according to the control strategies described in the next section.

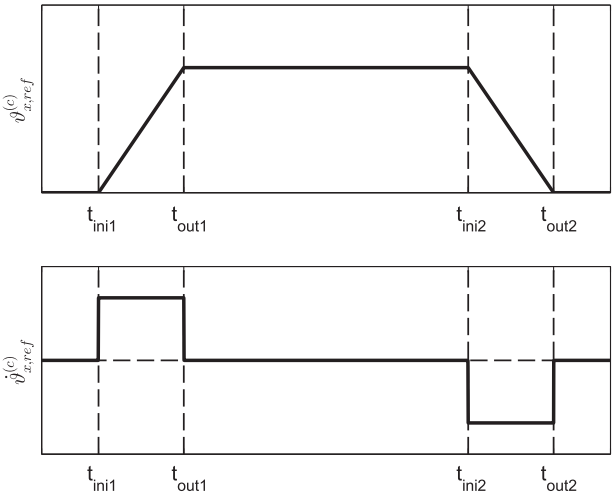

Fig. 3. Reference tilt angle and its time derivative along the curve.

4. Control strategies

The main objective of the control system is to track a reference carbody tilt angle $\vartheta_{x,ref}^{(c)}$, defined on the basis of the geometry of the curve being negotiated and of the vehicle speed. Assuming the vehicle to run at constant speed, the reference tilt angle results in a trapezoidal profile, with ramps occurring during the negotiation of the entry and exit transition spirals and a constant value in full curve (see Fig. 3).

Three alternative control strategies are considered:

- feed-forward + PID feed-back (PID);
- feed-forward + PID feed-back + Sky-Hook damping (PIDSH);
- Linear Quadratic controller with integral feedback (LQ).

4.1. Feed-forward + PID feed-back regulator

This is the simplest control strategy considered: the command to the servo-valve u_s is defined as the sum of a feed-forward contribution u_{FF} and of a PID feed-back term u_{FB} (see Fig. 4). The feed-forward contribution, representing the main contribution to

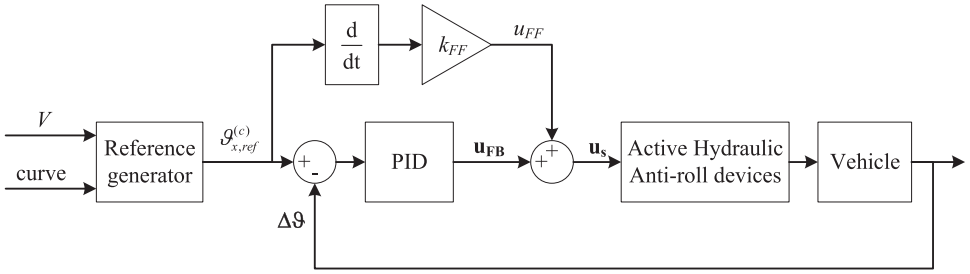

Fig. 4. Block diagram of the feed-forward + PID feed-back regulator.

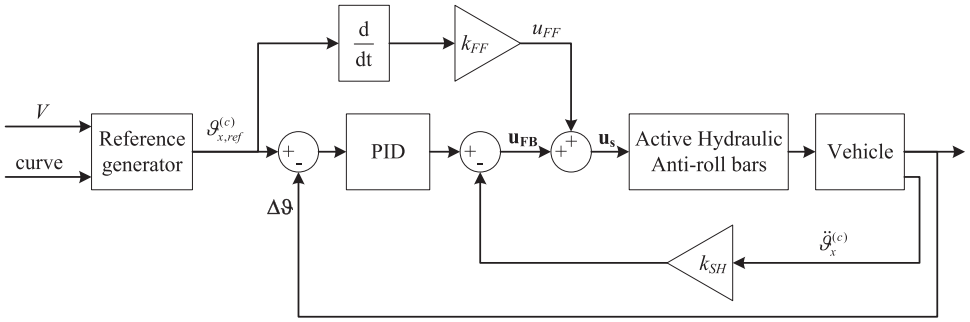

Fig. 5. Block diagram of the feed-forward + PID regulator with Sky-Hook damping (PIDSH).

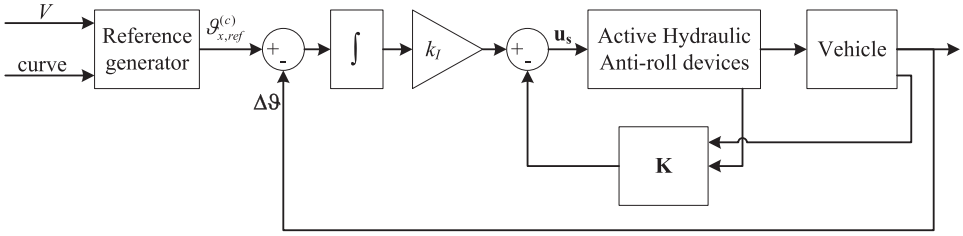

Fig. 6. Block diagram of the Linear Quadratic regulator with integral action (LQ).

the control action, aims to provide a fast response of the actuated system, whereas the feed-back contribution aims to compensate the effect of the simplifying assumptions used to define the feed-forward component and the effect of the external disturbances mainly caused by track irregularity.

In first approximation, i.e. by considering the fluid as completely incompressible and neglecting piston leakages, the hydraulic system behaves as an integrator. For this reason, the feed-forward contribution u_{FF} is defined as proportional to the time derivative of the reference carbody tilt $\vartheta_{x,ref}$ and takes a constant non-zero value in the transition spirals and zero value in full curve owing to the shape of the reference tilt profile (see Fig. 3).

For the feed-back contribution u_{FB} a PID regulator is adopted, acting on the error between the reference tilt angle and the relative carbody-bogie roll $\Delta\vartheta_x$:

$$u_{FB} = k_P\left(\vartheta^{(c)}_{x,ref} - \Delta\vartheta_x\right) + k_D\left(\dot{\vartheta}^{(c)}_{x,ref} - \Delta\dot{\vartheta}_x\right) + k_I\int\left(\vartheta^{(c)}_{x,ref} - \Delta\vartheta_x\right)dt \quad (13)$$

with

$$\begin{aligned}\Delta\vartheta_x &= \vartheta^{(c)}_x - \vartheta^{(l)}_x \quad \text{for the leading bogie}\\ \Delta\vartheta_x &= \vartheta^{(c)}_x - \vartheta^{(t)}_x \quad \text{for the trailing bogie}\end{aligned} \quad (14)$$

The regulator gains k_P, k_D and k_I in (13) are defined by means of Genetic Algorithm based optimisation, as described in Section 5.1. Note that, in order to use a practical measure, the error in (13) is defined based on the carbody roll rotation relative to the bogie instead of relative to the top-of-rail plane. As a consequence, the feedback command u_{FB} is different for the leading and trailing bogies. For the same reason, a positioning error due to the roll rotation of the bogies is expected; this error is however small owing to the considerable stiffness of the primary suspension.

4.2. Feed-forward + PID feed-back regulator + Sky-Hook damping

Tilting capabilities should be introduced without increasing, or even reducing, the level of carbody vibration in response to the transient excitation induced by curve negotiation and to track irregularities. For this reason, a second control strategy is considered, which is the same as the one described in Section 4.1 with the addition of Sky-Hook damping (see Fig. 5).

Thanks to the pseudo-integrator introduced by the hydraulic system, the sky-hook damping contribution can be defined as proportional to the carbody absolute roll acceleration $\ddot{\vartheta}^{(c)}_x$:

$$u_{FB} = k_P\left(\vartheta^{(c)}_{x,ref} - \Delta\vartheta_x\right) + k_D\left(\dot{\vartheta}^{(c)}_{x,ref} - \Delta\dot{\vartheta}_x\right) + k_I\int\left(\vartheta^{(c)}_{x,ref} - \Delta\vartheta_x\right)dt - k_{SH}\ddot{\vartheta}^{(c)}_x \quad (15)$$

thus requiring the additional measure of $\ddot{\vartheta}^{(c)}_x$ besides the carbody-roll relative rotations $\Delta\vartheta_x$ measured on the two bogies. The gain k_{SH} associated with the sky-hook damping contribution is added to the parameters to be defined through GA optimisation (Section 5.1).

4.3. Linear Quadratic regulator with integral feedback (LQ)

The third and last control strategy considered consists of a Linear Quadratic regulator with integral feed-back action (see Fig. 6).

The integral gain k_I and the gain matrix $\mathbf{K}$ are computed by solving an infinite horizon LQ problem, that consists of minimising the following cost function:

$$\tilde{J} = \frac{1}{2}\int_0^{\infty} (\tilde{\mathbf{x}}^{\mathrm{T}}\mathbf{Q}\tilde{\mathbf{x}} + \mathbf{u}_s^{\mathrm{T}}\mathbf{R}\mathbf{u}_s)dt \tag{16}$$

where the augmented state vector $\tilde{\mathbf{x}} = [\mathbf{x}_{hc} \quad \mathbf{z}]^{\mathrm{T}}$ is composed of the state vector $\mathbf{x}_{hc}$ of the hydraulic system and of the carbody, neglecting the bogie dynamics, and of the integrals of the error $\mathbf{z} = \int(\vartheta_{x,ref}^{(c)} - \Delta\vartheta_x)dt$.

The weight matrices $\mathbf{Q}$ and $\mathbf{R}$ are defined as diagonal matrices. In this case, the diagonal terms of these matrices are the parameters chosen by means of GA optimisation. The implementation of LQ requires measurement of carbody motion, relative to the bogie, and of the pressures inside the hydraulic circuit.

5. Simulation results

In this section, the mathematical model of the actuated vehicle defined in Section 3 is used to define the gains of the regulators introduced in Section 4 by means of Genetic Algorithm optimisation. Then, the performance of the actuated vehicle is assessed by numerical simulation. The vehicle considered for this assessment is a fictitious but realistic high-speed vehicle. Table 1 reports the parameters of the active hydraulic suspension and some main parameters of the vehicle considered. Both regulator gain optimisation and performance assessment are carried out considering one single high-speed curve geometry with radius 5500 m and cant 105 mm, which is very common in the Italian high-speed network and represents for this scenario the most demanding case for testing the performance of active suspension.

5.1. Optimisation of regulator gains

Optimisation was used to find the most suitable control parameters. Since the solution space is large, reasonably full of local optima and non-linear, a global optimisation method was preferred to local ones. Genetic algorithms have proven to be a suitable tool for regulator optimisation in general (Fleming & Purshouse, 2002) and specifically for active suspensions in ground vehicles (Baumal, McPhee, & Calamai, 1998; He & McPhee, 2005; Tsao & Chen, 2001).

Genetic algorithms can be used to optimize either a single fitness function or multiple ones: in the first case they are called single objective genetic algorithms (SGA), in the second multi-objective genetic algorithms (MOGA). The second option is adopted here, leading to the definition of Pareto front solutions among which the most appropriate set of regulator gains are identified. Therefore, four fitness functions were chosen for the optimisation:

1. maximum absolute error in trajectory tracking;
2. P_{CT} index for seated passengers:, this is a measure of ride comfort on curve transitions, adopted especially for tilting trains, and is defined as a non-linear function of the maximum lateral acceleration, the maximum lateral jerk and the maximum carbody roll speed perceived by the passengers during the negotiation of transition curves (CEN EN 12299, 2009), with higher P_{CT} values being associated with a greater probability of passengers suffering motion sickness;
3. r.m.s. of the lateral vibration perceived by seated passengers;
4. r.m.s. of actuation command given to servo-valve.

Table 1
Parameters of the active suspension and main parameters of the rail vehicle.

Variable name	Symbol	Value
Fluid volume in each main branch	V_0	1.5×10^{-2} m^3
Area of the piston	A	1.963×10^{-3} m^2
Oil bulk modulus	β	1.1×10^9 Pa
Supply pressure	p_S	198×10^5 Pa
Return pressure	p_R	2×10^5 Pa
Distance between actuators	b	2.57 m
Carbody mass		40,700 kg
Carbody roll moment of inertia		8.8×10^5 kg m^2

The first objective defines the reference signal to be followed accurately during curve negotiation and the reduction of the quasi-static lateral acceleration in curve to be effectively achieved. The second and third objectives are meant to ensure appropriate ride comfort level for passengers, with reference to the negotiation of curve transition and to the response to track irregularity respectively. The last objective ensures that energy consumption entailed by active carbody tilt is kept within acceptable limits. It is worth pointing out that, while all of the first three objectives relate to ride comfort for passengers, they cover different aspects that can be conflicting, thus requiring the definition of an appropriate trade-off when setting tilt control, as also pointed out in Zolotas, Goodall, and Halikias (2007). This is why these objectives are considered separately in the optimisation.

The variables to which the multi-objective optimisation is applied are the regulator gains, i.e. the proportional, integral and derivative gains for the PID regulator, the same three parameters plus a skyhook damping gain for the PIDSH strategy and the six diagonal elements in the weight matrix $\mathbf{Q}$ of the LQ regulator.

The algorithm chosen for the optimization of the regulators is the non-sorting genetic algorithm II (NSGA-II) (Deb, Agrawal, Pratap, & Meyarivan, 2000), one of the best-performing MOGA approaches in terms of convergence speed and elitism (ability of preserving the best individuals).

Each generation of the genetic algorithm process is ranked against all four fitness functions, and a multi-dimensional Pareto frontier is defined as approximated by the discrete population formed by the non-dominated individuals in the considered generation.

The genetic algorithm operators were chosen empirically by trial and error. The population size was 150 individuals for all the regulators. Selection was tournament-based, two individuals at a time, without replacement; crossover was single point and polynomial mutation had a 10% probability. The optimisation was terminated at 150 generations, which assured convergence to a stable Pareto front approximation.

The NSGA-II algorithm produced a set of optimal solutions belonging to a 4-dimension Pareto surface. Figs. 7–9 show some of the projections in 2-dimension of the solutions found, for the PID, PIDSH and LQ regulators respectively. For the PID regulator (Fig. 7), significant positive correlation is observed for the tracking error and the P_{CT} index, so that a decrease of the tracking error generally leads also to an improved level of ride comfort. The r.m.s. lateral acceleration (not displayed for the sake of brevity) shows limited variations across the set of identified optimal solutions. Moreover, the r.m.s. of the actuation command is increasing for decreasing P_{CT} and tracking error, showing as expected that more actuation energy is required to improve the performance of the active suspension. In the central and right plots of Fig. 7a “knee” is observed corresponding to a P_{CT} value of 2.4, a tracking error of 7.7 mrad and an r.m.s. of actuation of approximately 0.028 V. On this point, further improvements of the PCT and tracking error can be obtained only by applying a much larger actuation.

An examination of the set of optimal solutions found for the PIDSH regulator (cf. Fig. 8), shows it is possible to achieve lower P_{CT} values (and hence improved ride comfort levels) compared to the PID regulator, at the price of an increase of the actuation

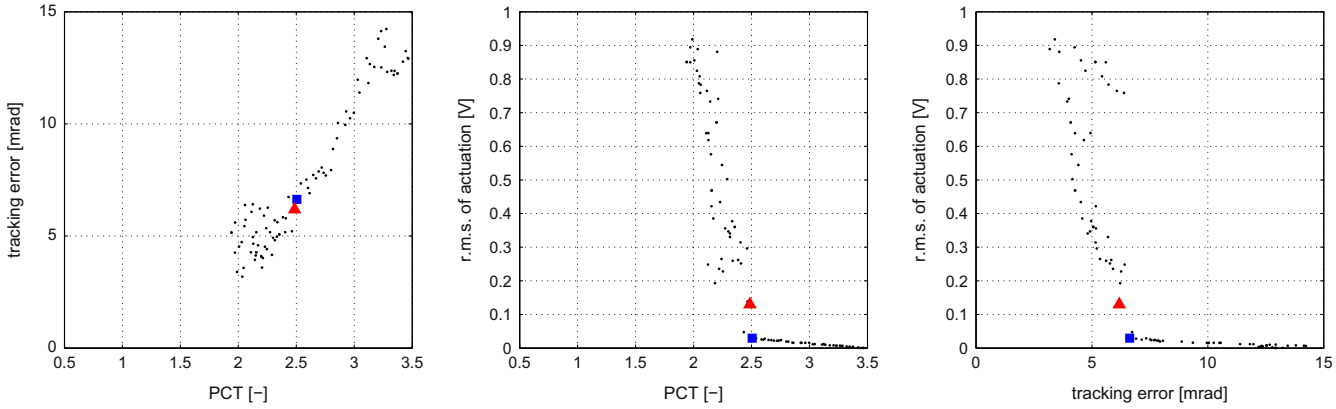

Fig. 7. 2-D projections of the optimal surface for the PID controller.

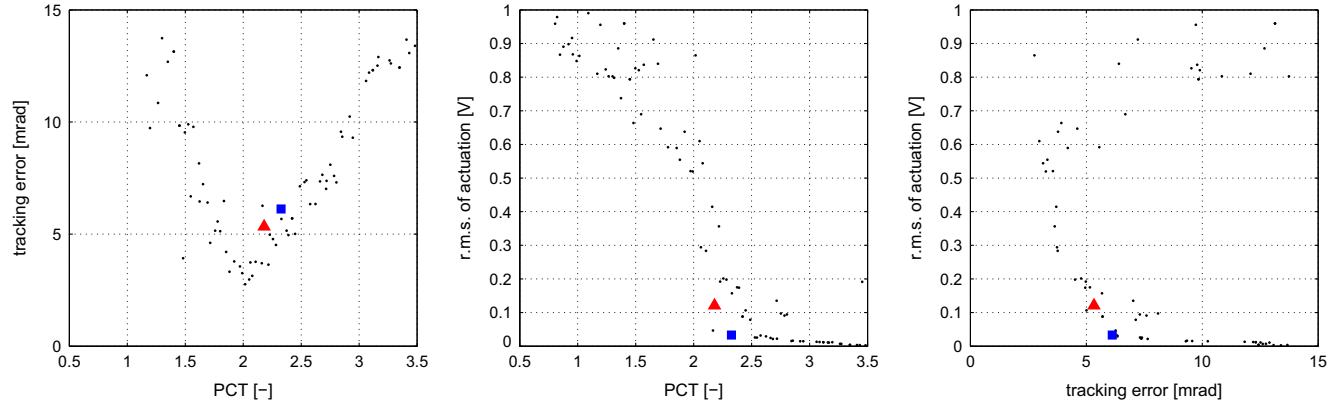

Fig. 8. 2-D projections of the optimal surface for the PIDSH controller.

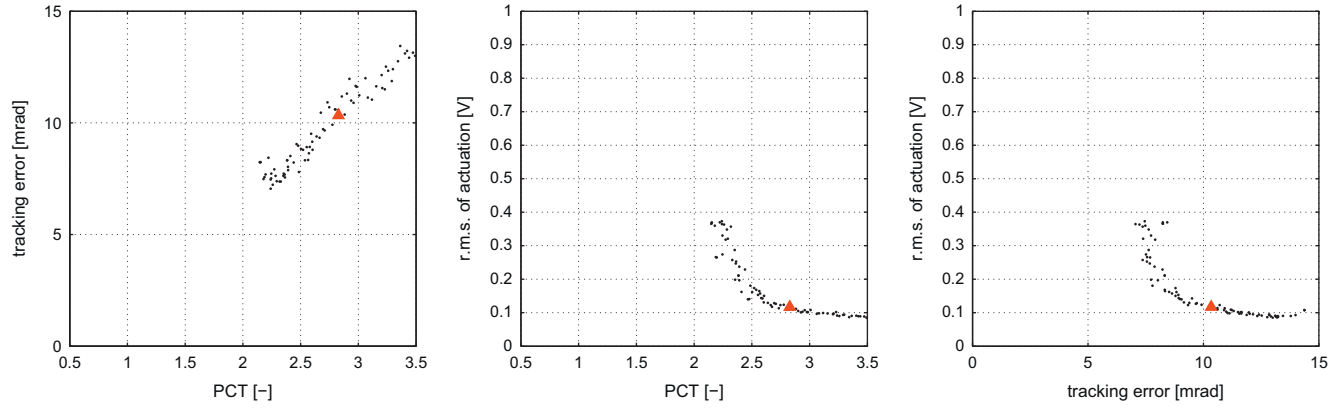

Fig. 9. 2-D projections of the optimal surface for the LQ controller.

command r.m.s. In this case, the trend of the PCT index with the tracking error is not monotone and, compared to the PID regulator, larger tracking errors need to be incurred to achieve P_{CT} values in the range of 1.5 or lower.

Finally, for the LQ regulator (cf. Fig. 9), slightly higher P_{CT} and tracking error values are obtained compared with the other two regulators. As will be further discussed in Section 5.2, this is mainly because the LQ regulator does not include the feed-forward contribution u_{FF}, and hence performance in terms of reference tracking and ride comfort is affected by a longer delay in controller action during the negotiation of the entry transition spiral.

In conclusion, five configurations from the GA optimisation of the three controllers are retained for further analysis in Section 5.2. To this end, two levels of r.m.s. of actuation are chosen, the lower one corresponding to the "knee" observed in Fig. 7 and the second one approximately three times greater. Then, for each regulator, the optimal gain set providing the minimum P_{CT} value for the chosen level of actuation is selected. For the LQ regulator, no solution is available for the lower level of actuation, and hence only one configuration is considered, corresponding to the higher r.m.s. of actuation. The configurations selected for further analysis are shown in Figs. 7–9 by square markers (low actuation level) and triangular markers (high actuation level).

5.2. *Analysis of the optimised controllers*

To evaluate and compare the effect of the three control techniques, a pole plot is shown in Fig. 10 for the optimised

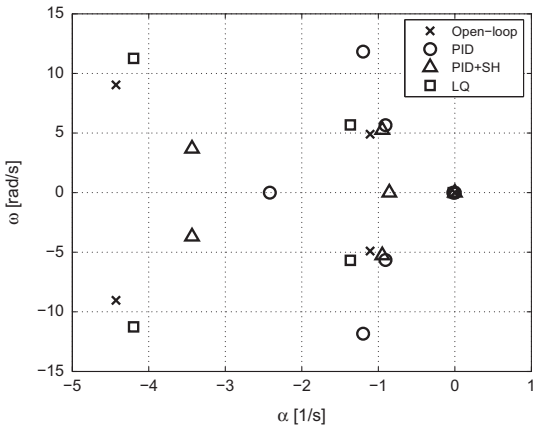

Fig. 10. Poles location for the passive and controlled systems.

controllers. Conclusions can also be drawn on the stability properties of the optimised controllers. This point is especially relevant for the PID with sky-hook controller, since a sky-hook controlled suspension can become unstable in real active isolation systems (Elliott, Serrand, & Gardonio, 2001). The pole plot is shown for a 4 degree-of-freedom half-vehicle model considering the lateral displacement and roll rotation of the half car body and of one bogie. For clarity, only the poles representing the low-frequency behaviour of the vehicle are shown.

All the optimised controllers were considered in the analysis, but for the sake of brevity Fig. 10 shows only those with a higher command r.m.s. Crosses represent the dynamics of the vehicle actuated in open loop: a real pole can be seen close to the origin of the diagram and is associated with the dynamic of the hydraulic anti-roll bar. Two complex conjugate pole couples describe the first lateral and first roll mode of the suspension. The two poles situated approximately at 5 rad/s are associated with the lateral vibration of the carbody, while the other two at 9 rad/s are related to the roll motion of the carbody.

The poles of the vehicle actuated in closed loop show an additional pole due to the dynamics of the low-pass filter. The poles of the optimised solution with the PID controller, shown by circles, are close to those of the vehicle actuated in open loop as far as the lateral vibration of the car body is concerned, but show a significantly lower real part and hence lower damping for car body roll. The poles of the PID with sky-hook damping optimised controller are shown as triangles. The real and imaginary part of the poles associated with lateral car body motion are again close to those of the vehicle actuated in open loop, while the poles associated with car body roll have lower real and imaginary parts, showing mainly a reduction of the natural frequency for approximately the same level of damping.

Finally, the poles of the vehicle with LQ controller (squares) show an increased damping of the lateral car body motion while preserving car body roll dynamics similar to those of the vehicle actuated in open loop.

Some conclusions can be drawn from the analysis of the pole diagram: all the optimised controllers provide acceptable stability margins, the lateral vibration of the car body is only weakly affected by the type of controller while larger differences are found in terms of roll car body motion. Finally, the stability of the PID with sky-hook controller is not seriously compromised by the flexibility of the primary suspension, as could have been expected from earlier literature (Elliott et al., 2001). This is because on railway vehicles the primary suspension is much stiffer than the secondary suspension, so the effect of its compliance on stability is less.

5.3. *Performance evaluation for the optimised regulators*

This section reports the results of time domain simulations for selected regulator configurations considering the active vehicle running at 340 km/h along a curve having the same geometry already considered in Section 5.1. For comparison, the behaviour of a conventional passive vehicle running at 300 km/h is also considered.

Fig. 11 shows the roll angle of the carbody relative to the top-of-rail plane as a function of the vehicle position along the track, considering four different vehicle configurations: the passive vehicle (top left), and the active vehicle considering the three control strategies introduced in Section 4: PID (top right), PIDSH (bottom left) and LQ (bottom right). For all active vehicle configurations, results are shown for the gain configuration corresponding to the high level of r.m.s. of actuation.

As concerns the dynamics of the passive vehicle, it can be seen that when the vehicle enters the curve the carbody begins to rotate outwards (positive values of the roll angle) owing to the inertial force. Considering instead the active vehicle, the carbody is actuated to follow the reference tilt angle, shown as a dotted line, directed towards the inside of the curve. It can be seen that all controllers are able to track the reference with good accuracy, although the LQ controller shows a delay which is due to the lack of the feed-forward contribution. As anticipated in Section 4, all regulators show a small steady state error in full curve because the error on carbody rotation is defined on the basis of the relative and not the absolute roll angle.

The lateral acceleration felt by the passengers is shown in Fig. 12 for the same vehicle configurations previously described. It is apparent that carbody tilt is able to adequately compensate for the larger cant deficiency caused in the active vehicle by the increase of speed. Furthermore, the PIDSH and LQ controllers are also able to compensate for the increased level of high-frequency excitation produced by track irregularity, which increases with the square of speed. The simpler PID controller is less efficient in reducing the high-frequency dynamic fluctuations of the acceleration signal, resulting in slightly worse ride comfort levels compared with the other two control strategies, as further discussed below.

The ride comfort indices (P_{CT} and r.m.s. of the lateral acceleration) and the average power (per bogie) required for actuating the carbody are compared in Table 2 for the vehicle with active suspension running at 340 km/h and for the passive vehicle running at 300 km/h. Active tilt control improves the P_{CT} despite the increase of speed, while r.m.s. lateral acceleration is only slightly increased. It can be concluded that the active suspension allows the curve to be negotiated 40 km/h faster with comparable ride comfort levels.

As far as the comparison of alternative regulator configurations is concerned, for the PID regulator only a marginal improvement of the P_{CT} index is obtained if the gain settings corresponding to a higher level of actuation are used, at the expense of more power being required for actuation. On the other hand, for the PIDSH regulator performance can be improved significantly in terms of both comfort indices by increasing actuation intensity. The LQ regulator is effective in reducing the components of carbody vibration generated by track irregularities and hence r.m.s. lateral acceleration, but is less effective than the other two regulators in terms of P_{CT} value, owing to the delay in actuation mentioned above. Overall, the PIDSH regulator with high actuation level produces the best ride comfort performance, with an acceptable level of actuation power.

Simulations also showed that the use of active tilt (in conjunction with an active lateral secondary suspension) does not cause running safety issues: the track shift forces and the derailment and overturning coefficients were verified to remain well within the admissible ranges, despite the increase of speed from 300 to 340 km/h.

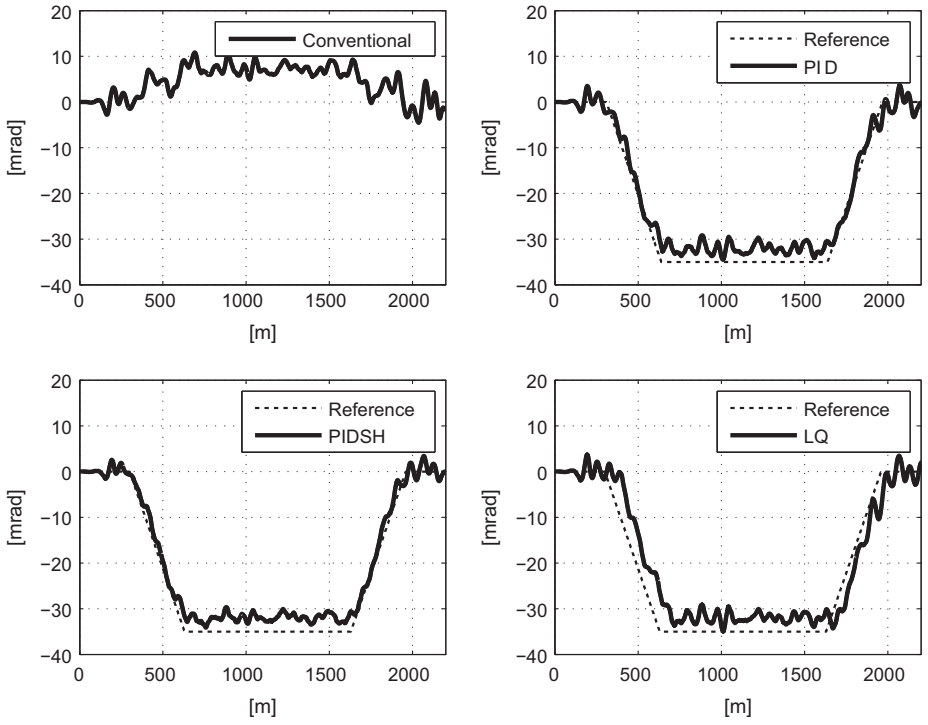

Fig. 11. Time history of the carbody roll rotation. Top left: passive vehicle 300 km/h. Top right: PID regulator, 340 km/h. Bottom left: PIDSH regulator, 340 km/h. Bottom right: LQ regulator, 340 km/h.

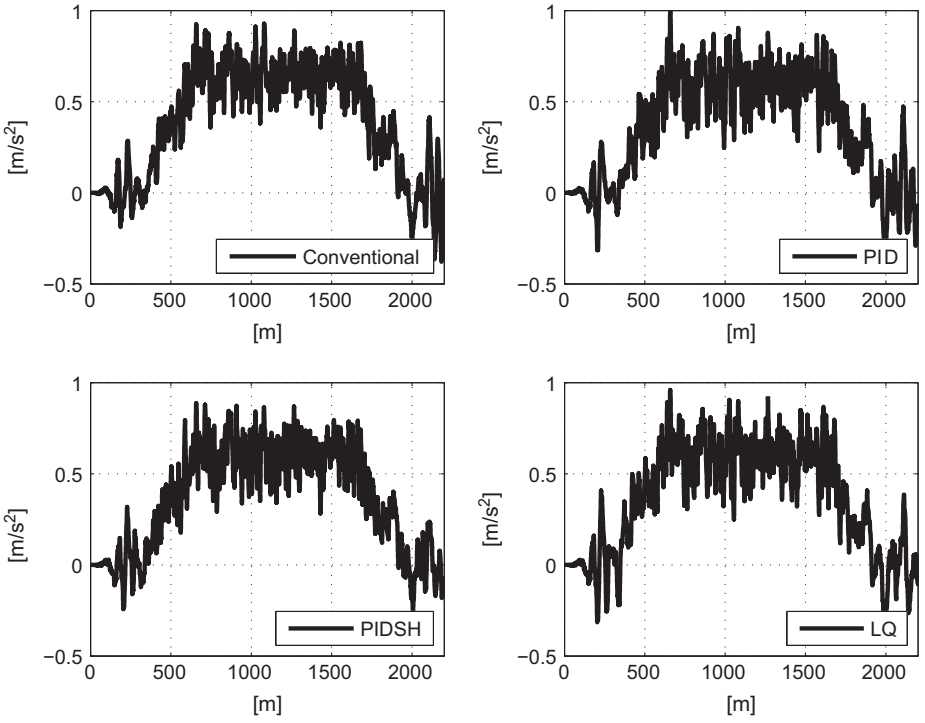

Fig. 12. Time history of the lateral acceleration perceived by passengers. Top left: passive vehicle 300 km/h. Top right: PID regulator, 340 km/h. Bottom left: PIDSH regulator, 340 km/h. Bottom right: LQ regulator, 340 km/h.

6. Conclusions

This paper proposed a novel concept for an active hydraulic anti-roll bar for use in high speed railway vehicles, with the aim of applying a limited amount of carbody tilt and reducing the exposure of passengers to non-compensated lateral acceleration in curves. Three control strategies were defined for the active suspension, and their parameters were chosen based on multi-objective Genetic Algorithm optimisation using a multi-body model of the actuated vehicle. Four objective functions were considered in the optimisation process, representing quantitative measurements of the tracking error, ride comfort and energy required for actuation.

Table 2
Comparison of the comfort indexes and power required for actuation.

	Speed [km/h]	P_{CT} (seated passengers) [dimensionless]	r.m.s. lateral acceleration [m/s^2]	r.m.s. of power required for actuation (per bogie) [kW]
Passive	300	2.98	0.159	–
PID (low actuation level)	340	2.51	0.200	0.536
PID (high actuation level)	340	2.49	0.222	0.996
PIDSH (low actuation level)	340	2.33	0.194	0.548
PIDSH (high actuation level)	340	2.18	0.183	0.940
LQ (high actuation level)	340	2.83	0.188	0.764

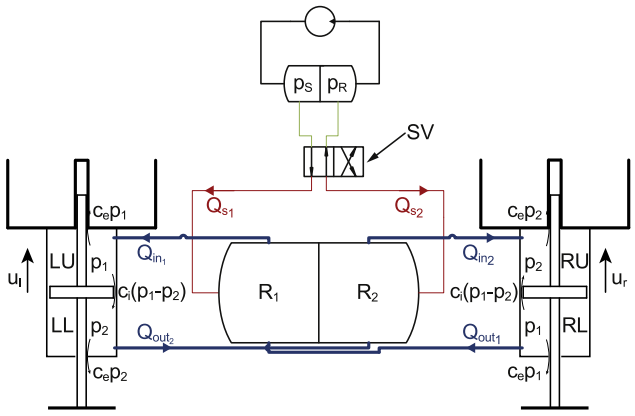

Fig. A1. Fluid flow rates and piston displacements in the active suspension.

Considering the case of a vehicle running on a typical curve in a high-speed railway network, simulation results show that the active suspension permits an increase in vehicle speed from 300 km/h to 340 km/h for the same or improved ride comfort. The mean power required to operate the active suspension is in the range of 0.5–1.0 kW per bogie, which is fully feasible for the application envisaged here. The control strategy based on feed-forward + PID feed-back with sky-hook damping provides the best performance in terms of ride comfort for an acceptable actuation power requirement. The LQ regulator is effective in mitigating carbody vibration induced by track irregularity, but its overall performance is affected by significant actuation delay during the negotiation of curve transitions.

Further work is planned on the integration of active tilt and active lateral control for the secondary suspension and to investigate the rejection of disturbances generated by track irregularity in a wider frequency range, also considering the effects of carbody deformability.

Appendix A

In this appendix, the details of derivation of Eqs. (1) and (2) are reported. Fig. A1 shows the fluid flow rates in the active suspension hydraulic circuit.

For a compressible fluid, the bulk modulus β is defined as (Merritt, 1967)

$$\beta = \rho_0 \left.\frac{\partial p}{\partial \rho}\right|_{\rho_0} \tag{A.1}$$

Considering mass conservation for each actuator chamber under the assumption of partially compressible fluid results in the following equations:

$$Q_{in_1} - c_i(p_1 - p_2) - c_e p_1 = -A\dot{u}_l + \frac{V_A - Au_l}{\beta}\dot{p}_1 \tag{A.2}$$

$$-Q_{out_1} - c_i(p_1 - p_2) - c_e p_1 = +A\dot{u}_r + \frac{V_A + Au_r}{\beta}\dot{p}_1 \tag{A.3}$$

$$Q_{in_2} + c_i(p_1 - p_2) - c_e p_2 = -A\dot{u}_r + \frac{V_A - Au_r}{\beta}\dot{p}_2 \tag{A.4}$$

$$Q_{out_2} + c_i(p_1 - p_2) - c_e p_2 = A\dot{u}_l + \frac{V_A + Au_l}{\beta}\dot{p}_2 \tag{A.5}$$

where V_A is the volume of the actuator chambers in the reference configuration, Q_{in_1}, Q_{out_1}, Q_{in_2}, and Q_{out_2} are the fluid flow rates shown in Fig. A1, and all other symbols are introduced in Section 3.

Furthermore, mass conservation for the two reservoirs leads to the following two equations:

$$-Q_{in_1} + Q_{out_1} + Q_{s_1} = \frac{V_R}{\beta}\dot{p}_1 \tag{A.6}$$

$$-Q_{in_2} + Q_{out_2} + Q_{s_2} = \frac{V_R}{\beta}\dot{p}_2 \tag{A.7}$$

with V_R the volume of each reservoir.

Introducing (A.6) in the sum of (A.2) and (A.3) gives Eq. (1). In the same way, introducing (A.7) in the sum of (A.4) and (A.5) gives Eq. (2).

References

Alfi, S., Bruni, S., Diana, G., Facchinetti, A., & Mazzola, L. (2011). Active control of airspring secondary suspension to improve ride quality and safety against crosswind. *Proceedings of the Institution of Mechanical Engineers, Part F: Journal of Rail and Rapid Transit*, *225*(1), 84–98.

Baumal, A. E., McPhee, J. J., & Calamai, P. H. (1998). Application of genetic algorithms to the design optimization of an active vehicle suspension system. *Computer Methods in Applied Mechanics and Engineering*, *163*(1–4), 87–94.

Braghin, F., Bruni, S., & Diana, G. (2006). Experimental and numerical investigation on the derailment of a railway wheelset with solid axle. *Vehicle System Dynamics*, *44*(4), 305–325.

Bruni, S., Collina, A., Diana, G., & Vanolo, P. (1999). Lateral dynamics of a railway vehicle in tangent track and curve: Tests and simulation. *Vehicle System Dynamics*, *33*(S), 464–477.

Bruni, S., Goodall, R. M., Mei, T. X, & Tsunashima, H. (2007). Control and monitoring for railway vehicle dynamics. *Vehicle System Dynamics*, *45*(7), 743–779.

CEN EN 12299 (2009). *Railway applications – Ride comfort for passengers – Measurement and evaluation*, Brussels.

Colombo, E. F., Di Gialleonardo, E., Facchinetti, A., & Bruni, S. (2013). Study of an active hydraulic anti-roll device for high-speed railway vehicle. In *Proceedings of the 23rd IAVSD symposium*.

Deb, K., Agrawal, S., Pratap, A., & Meyarivan, T. (2000). A fast elitist non-dominated sorting genetic algorithm for multi-objective optimization: NSGA-II, parallel problem solving from nature PPSN VI. *Lecture Notes in Computer Science*, *1917*, 849–858.

Di Gialleonardo, E., Braghin, F., & Bruni, S. (2012). The influence of track modelling options on the simulation of rail vehicle dynamics. *Journal of Sound and Vibration*, *331*(19), 4246–4258.

ERRI: B176/3 (1993). *Benchmark problem — Results and assessment*, B176/DT290, Utrecht.

Elliott, S. J., Serrand, M., & Gardonio, P. (2001). Feedback stability limits for active isolation systems with reactive and inertial actuators. *Journal of Vibration and Acoustics*, *123*(2), 250–261.

Facchinetti, A., Di Gialleonardo, E., Resta, F., Bruni, S., & Brundisch, V., (2011). Active control of secondary airspring suspension. In *Proceedings of the 22nd IAVSD symposium*.

Fleming, P. J., & Purshouse, R. C. (2002). Evolutionary algorithms in control systems engineering: A survey. *Control Engineering Practice*, *10*(11), 1223–1241.

Goodall, R. M. (2011). Control engineering challenges for railway trains of the future. *Measurement and Control*, *44*(1), 16–24.
Goodall, R. M., Bruni, S., & Facchinetti, A. (2012). Active control in railway vehicles. *International Journal of Railway Technology*, *1*(1), 57–85.
He, Y., & McPhee, J. (2005). Multidisciplinary design optimization of mechatronic vehicles with active suspensions. *Journal of Sound and Vibration*, *283*(1–2), 217–241.
Merritt, H. E. (1967). *Hydraulic control systems*. New York: John Wiley & Sons.
Nakakura, Y., & Hayakawa, K. (2009). *The body inclining system of the series N700 Shinkansen*. In *Proceedings of STECH'09 conference*.
Pearson, J. T., Goodall, R. M., & Pratt, I. (1998). Control system studies of an active anti-roll bar tilt system for railway vehicles. *Proceedings of the Institution of Mechanical Engineers, Part F: Journal of Rail and Rapid Transit*, *212*(1), 43–60.
Persson, R., Goodall, R. M., & Sasaki, K. (2009). Carbody tilting – Technologies and benefits. *Vehicle System Dynamics*, *47*(8), 949–981.
Tanifuji, K., Koizumi, S., & Shimamune, R. (2002). Mechatronics in Japanese rail vehicles: Active and semi-active suspensions. *Control Engineering Practice*, *10*(9), 999–1004.
Tanifuji, K., Saito, M., Soma, H., Ishii, T., Kajitani, Y. (2009). Vibration suppression of air spring-type tilting vehicle running at high-speed on curved section overlapped with vertical curve. In *Proceedings of the 21st IAVSD symposium.*
Tsao, Y. J., & Chen, R. (2001). The design of an active suspension force controller using genetic algorithms with maximum stroke constraints. *Proceedings of the Institution of Mechanical Engineers, Part D: Journal of Automobile Engineering*, *215*(3), 317–327.
Zhang, N., Smith, W. A., & Jeyakumaran, J. (2010). Hydraulically interconnected vehicle suspension: Background and modelling. *Vehicle System Dynamics*, *48*(1), 17–40.
Zhou, R., Zolotas, A., & Goodall, R. M. (2011). Integrated tilt with active lateral secondary suspension control for high speed railway vehicles. *Mechatronics*, *21*(6), 1108–1122.
Zolotas, A., Goodall, R. M., & Halikias, G. D. (2007). Recent results in tilt control design and assessment of high-speed railway vehicles. *Proceedings of the Institution of Mechanical Engineers, Part F: Journal of Rail and Rapid Transit*, *221*(2), 291–312.